

Coronal Thick Target Hard X Ray Emissions and Radio Emissions

Jeongwoo Lee^{1,2}, Daye Lim², G. S. Choe², Kap-Sung Kim², and Minhwan Jang³

1. *Physics Department, New Jersey Institute of Technology, Newark, NJ 07102*

2. *School of Space Research, Kyung Hee University, Yongin 446-701, Korea*

3. *Department of Astronomy and Space Science, Kyung Hee University, Yongin 446-701, Korea*

ABSTRACT

Recently a distinctive class of hard X ray (HXR) sources located in the corona was found, which implies that the collisionally thick target model (CTTM) applies even to the corona. We investigated whether this idea can independently be verified by microwave radiations that have been known as the best companion to HXR. The study is made for the GOES M2.3 class flare occurred on 2002 September 9 that were observed by the Reuven Ramaty High Energy Solar Spectroscopic Imager (RHESSI) and the Owens Valley Solar Array (OVSA). Interpreting the observed energy dependent variation of HXR source size under the CTTM the coronal density should be as high as $5 \times 10^{11} \text{ cm}^{-3}$ over the distance up to $12''$. To explain the cut-off feature of microwave spectrum at 3 GHz, we however, need density no higher than $1 \times 10^{11} \text{ cm}^{-3}$. Additional constraints need to be placed on temperature and magnetic field of the coronal source in order to reproduce the microwave spectrum as a whole. Firstly, a spectral feature called the Razin suppression requires the magnetic field in a range of 250–350 gauss along with high viewing angles around 75° . Secondly, to avoid excess fluxes at high frequencies due to the free-free emission that were not observed, we need a high temperature $\geq 2 \times 10^7 \text{ K}$. These two microwave spectral features, Razin suppression and free-free emissions, become more significant at regions of high thermal plasma density and are essential for validating and for determining additional parameters for the coronal HXR sources.

Subject headings: Sun: flares — Sun: X-rays, gamma rays — radio emission

1. INTRODUCTION

Observations of Hard X-ray (HXR) bursts with the Ramaty High Energy Solar Spectroscopic Imager (RHESSI) have produced a number of new properties of high energy electrons accelerated during solar flares. One of its recent discoveries is a distinctive type of flares in which the bulk of

the HXR emission is from the coronal part of the loop (Veronig & Brown 2004; Sui et al. 2004; Krucker et al. 2008). For such sources, the corona can be considered as not only the site of particle acceleration, but act as a thick target, stopping the accelerated electrons before they can penetrate to the chromosphere. This is in contrast with the traditional idea of the collisional thick target model (CTTM) that was believed to apply only to the dense chromosphere. Veronig & Brown (2004) studied two events for which the coronal densities of the flaring loops were found sufficiently high to justify the CTTM. Xu et al. (2008) showed that for a certain group of events the observed coronal HXR source extent varies with photon energy as expected from a CTTM with an extended acceleration region in the coronal loop. The result not only serves as evidence for the coronal CTTM, but also allows estimates of the plasma density and longitudinal extent of the acceleration region. Guo et al. (2012a) have carried out a similar work but using the electron flux images instead of photon maps, as constructed by regularized spectral inversion of the visibility data in the count domain (Piana et al. 2007). Guo et al. (2012b) further related those interpretations to the number of particles within the acceleration region, the filling factor, and the specific acceleration rate in units of electron per second and per ambient electron. According to these studies those events with the coronal thick target HXR sources form an important (though small) class of solar flares for which acceleration parameters can directly be inferred.

If we plan to test the CTTM for coronal HXR sources using other radiations, microwave radiation should be the first choice, for its close relationship with HXR. Time profiles of microwave emissions tend to show a peak-to-peak correlation with HXR lightcurves, which led to the idea of the same population of electrons responsible for both radiations (e.g., Dulk 1985). Spatially both emissions should arise, at least, from the same magnetic loop or loop systems, but the location of each radiation maximum may differ along the loop as their radiation efficiencies differently respond to plasma parameters and magnetic field (e.g., Sakao 1996). We expect that microwave spectrum will be particularly important in relation to the studies of the coronal CTTM. The main microwave radiation mechanism, gyrosynchrotron radiation, has primarily served as a diagnostic for magnetic field and electron distribution. However, when thermal density is very high, two spectral features sensitive to density, the Razin suppression (Razin 1960) and free-free emission, become prominent. The Razin suppression refers to less efficient radiation in the presence of ambient medium compared with the radiation in vacuum, and the Razin frequency below which the effect is significant is given by $\nu_R \approx 20 n/B_\perp$ Hz where n is electron density in units of cm^{-3} and B_\perp is the transverse magnetic field component in gauss. The Razin suppression will thus be effective for the condition of thick target looptop HXR sources. The well-known free-free opacity is proportional to $n^2 T^{-1/2}$, with T , the plasma temperature. In addition, there is an *absolute* cut-off of microwave radiation at the plasma frequency which is a sole function of plasma density (see, e.g., Dulk 1985, Melrose 1980). With these features that become prominent at high density, a microwave spectrum should play a critical role in validating the CTTM applied to coronal sources.

In this Letter we compare the properties of a coronal HXR source with those of microwave source detected in an event which we consider a candidate for the coronal thick target source. The event is the 2002 September 9 flare occurred in NOAA AR 0105 and acquired GOES soft X-ray class M2.3. This event was observed by the Reuven Ramaty High-Energy Solar Spectroscopic Imager (RHESSI) and the Owens Valley Solar Array (OVSA), respectively, and is one of the rare events for which spatial and spectral information at both wavelengths is available for this type of study.

2. SPECTRA OF HXR and Microwaves

In Figure 1 we show the RHESSI and OVSA spectra during the 2002 September 9 flare. The top panel shows the spatially integrated RHESSI spectrum at a single time corresponding to maximum emission measure obtained using OSPEX in the SolarSoftWare (SSW). Ji et al. (2004) carried out the imaging spectroscopy for the same event. In their result and also in ours (Fig. 2), the RHESSI source appears to be a single source and the spectra obtained through OSPEX are indeed similar to those obtained from the imaging spectroscopy. As a characteristic feature, the spectrum shows steeply decreasing flux with increasing photon energy with spectral indices as high as $7 \leq \gamma \leq 8$. Such high index is typical for the events classified for the coronal thick target HXR sources (Guo et al. 2012ab, Xu et al. 2007). The spectral index γ will later be used to provide the information on electron energy distribution to the modeling of the HXR source loop and that of the microwave spectra. In spite of such a soft nonthermal component, a thermal component could still be identified and the maximum temperature is found to be $T \approx 2 \times 10^7 \text{K}$ at around 17:50 UT, close to what we infer from GOES soft X-ray data.

The bottom panel shows the total power microwave spectra for the 2002 September 9 flare at three selected times. This is one of the calibrated microwave spectra in the period of 2001-2003 that can be downloaded from the OVSA web site. Like the HXR spectra, these microwave spectra are also spatially integrated and include both R and L polarizations added together. They appear in a typical shape, but with rapidly falling fluxes toward decreasing frequencies, which can be a sign for the Razin suppression, and is suggestive of a high coronal density. The high frequency spectrum is steeply decreasing with increasing frequency, which is qualitatively consistent with the high photon spectral index of the RHESSI spectrum as found above. We may also note that the peak frequency of microwave spectrum does not change much in the course of the flare. Previously, Belkora (2007) claimed that such a feature may indicate the effect of the Razin suppression. It is thus qualitatively arguable that the spectral morphology of the OVSA spectra is supportive of the high coronal density required for the CTTM of the coronal HXR source.

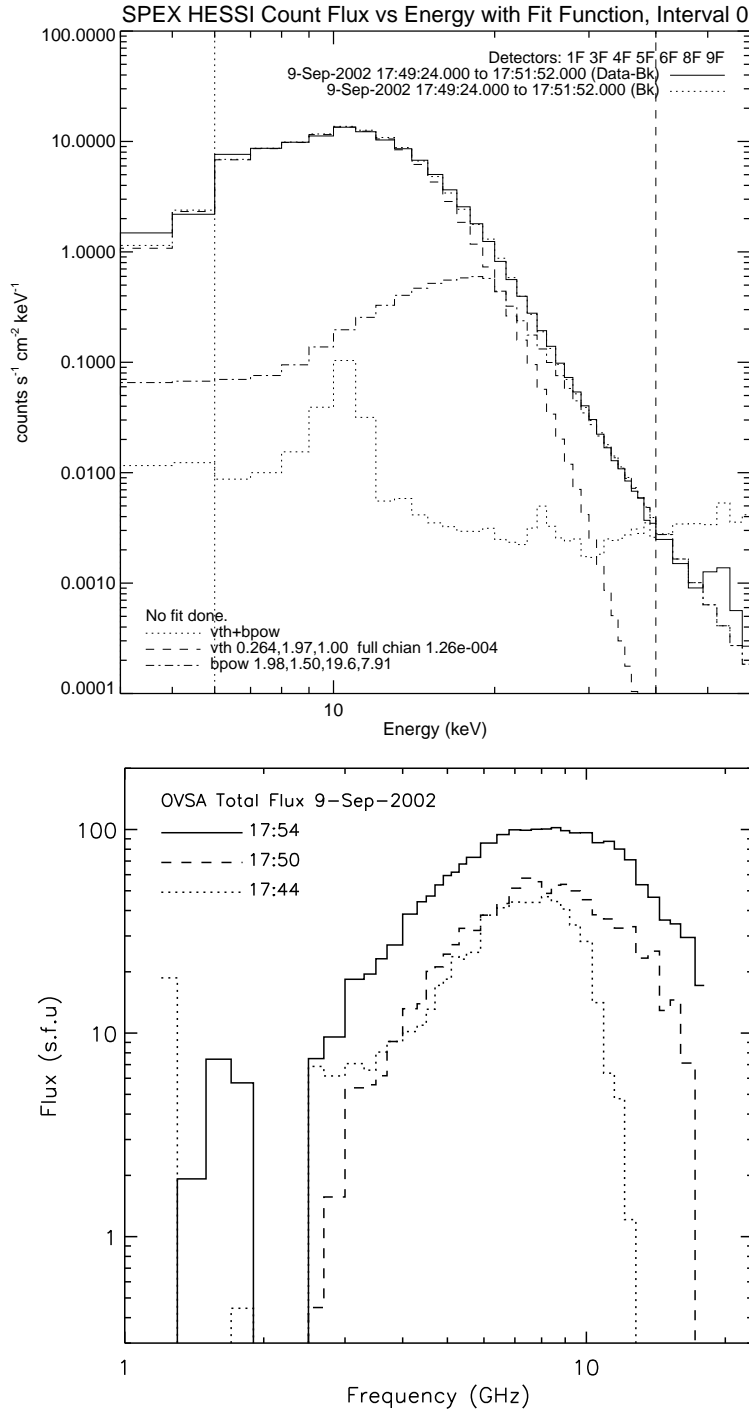


Fig. 1.— Upper panel: a RHESSI spectrum for the flare on 2002 September 9. Spectral fit is made for the interval, 17:49:23–17:51:53 UT. The thermal component of the spectrum (dashed histogram) has temperature of 1.97 keV and the nonthermal component (dot-dashed) has transition energy at 19.6 keV and spectral index $\gamma = 7.91$. The sum of the thermal and nonthermal components (solid histogram) and the background is also shown. Lower panel: the OVSA microwave spectra at three different time intervals as denoted are shown.

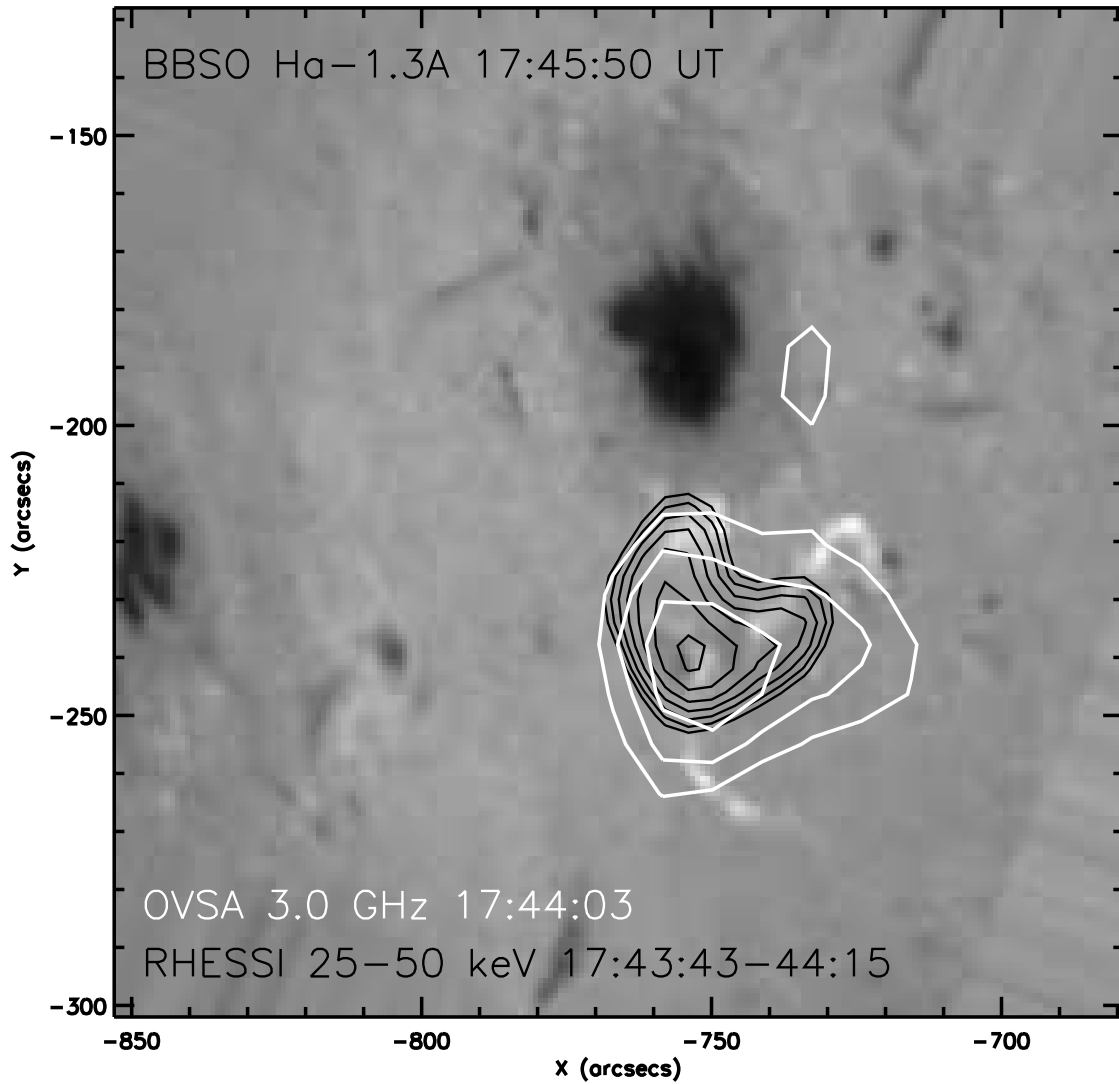


Fig. 2.— The 25-50 keV RHESSI source (black contours) and the OVSA microwave source (white contours) in comparison with the H α blue wing image (background greyscale image) from the BBSO. These images are chosen to be near one of the flare peak time 17:44 UT.

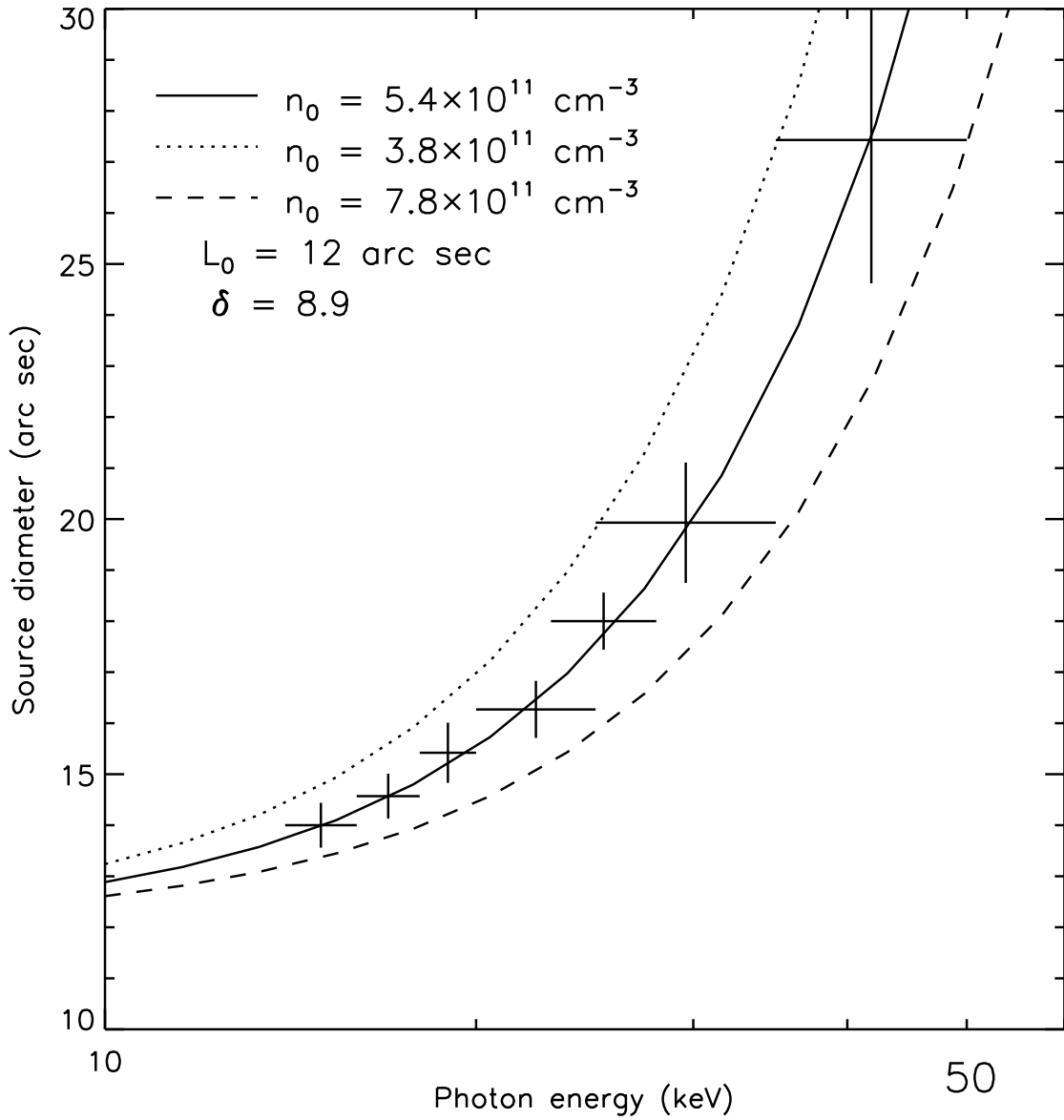


Fig. 3.— Model fits to the longitudinal dimension of the HXR source. We calculate models (lines) by varying ambient density n_0 and the initial length of the trap L_0 to fit the observed HXR source dimension (crosses) at seven photon energies.

3. HXR and Microwave maps

The OVSA imaging procedure is less known compared with that of the RHESSI. Since the OVSA uses many frequencies, all night observations of a quasar point source such as 3C84 are made several times a year, and are used to calibrate solar data obtained at nearby times. Daily calibration observations at selected frequencies are also made to provide corrections to the above calibration. The calibrated visibilities are fed into the *wimagr* program available in the SSW, after which the imaging can be performed in the procedure very similar to that of the Astronomical Image Processing System (AIPS).

Figure 2 shows HXR and microwave maps as contours on top of an $H\alpha$ off-band blue-wing image obtained from the Big Bear Solar Observatory (BBSO). Based on the steep HXR spectrum and the noise level (Fig. 1), the HXR imaging was performed below 50 keV. Within the energy range only single loop-top source was found. Microwave sources generally vary with frequency more significantly, but the centroid of 3.0 GHz microwave source is co-spatial with that of the 25–50 keV HXR source as shown in this figure. Both the HXR and microwave sources appear as a single source lying between the two $H\alpha$ kernels, and their morphologies change only a little with time (see, for more details on the morphology of this event, Ji et al. 2004 and Lee et al. 2006). We thus regard the HXR source as a loop-top coronal thick target source (cf. Veronig & Brown 2004). We followed the technique of Xu et al. (2007) to determine the source sizes using the Vis-Forward fitting and made a model fit to the observed HXR source size as a function of photon energy. As for the model, we actually used equation (5) of Guo et al. (2012b), which corresponds to Xu et al.’s (2007) model with an extended acceleration region of length, L_0 , uniformly filled with dense material of density n_0 . This model also includes the electron energy distribution with a power law index for which we use $\delta = \gamma + 1 = 8.9$ under the thick target bremsstrahlung approximation (Brown 1971). Figure 3 shows our fitting of the model to the observed HXR source size (symbols) at seven photon energies by varying n_0 and L_0 . We obtained $n_0 = (5.4 \pm 1.6) \times 10^{11} \text{ cm}^{-3}$ and $L_0 \approx 12''$ from these data.

4. Model Fits to the OVSA Spectra

We calculated a set of theoretical microwave spectra for comparison with the OVSA spectrum using the numerical code developed by Fleishman and Kuznetsov (2010), which includes full treatment of the Razin effect. In Figure 4 we show our search for the best set of model parameters with which we can reproduce the OVSA spectrum at the time of the maximum density ($\sim 17:50$ UT) chosen as a representative spectrum. In the top panel we first tried a modest density $2.1 \times 10^{10} \text{ cm}^{-3}$ and the same electron energy distribution derived from the RHESSI spectrum, i.e., $\delta = 8.9$, except that the electron energy distribution is assumed to extend up to 1 MeV. This model (shown as the dotted line

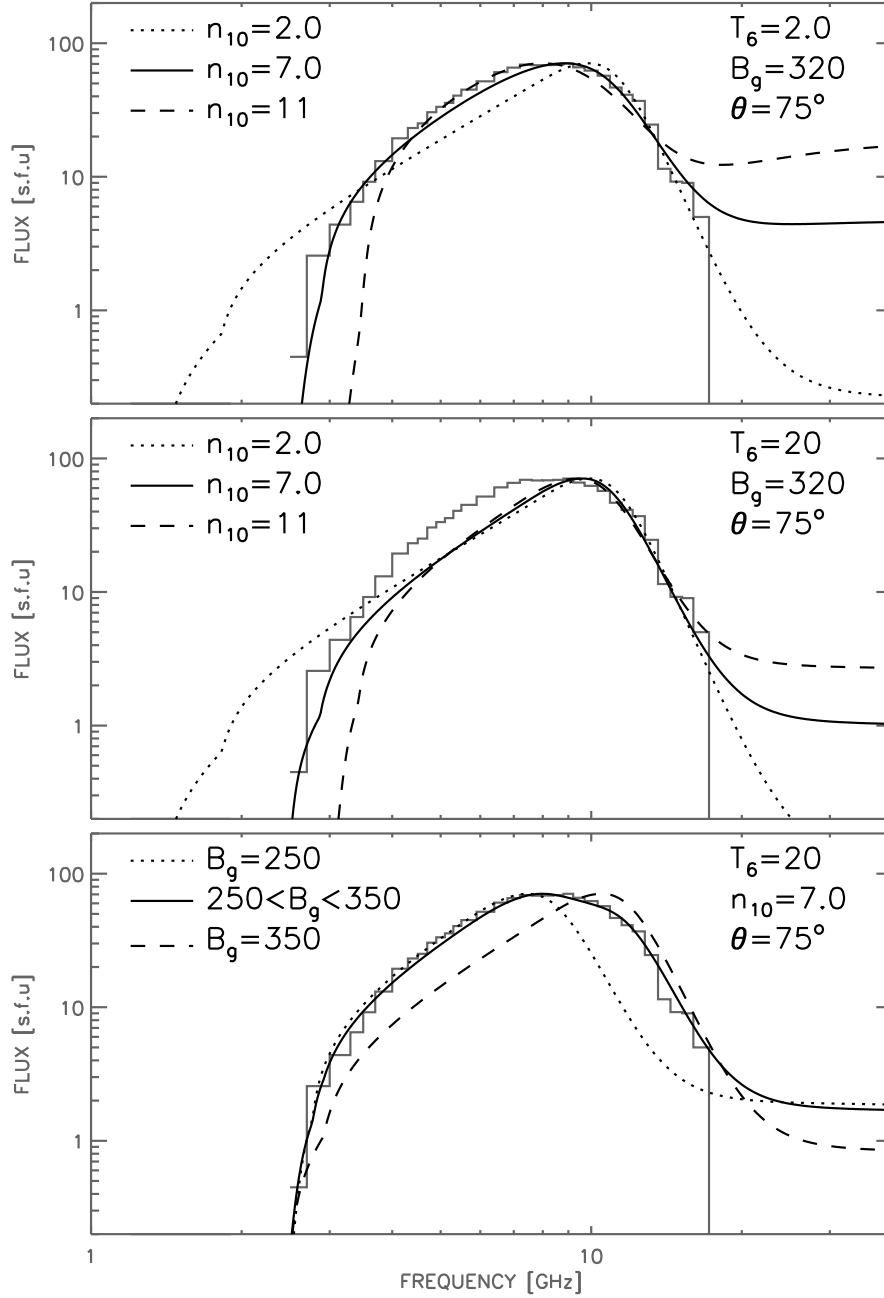


Fig. 4.— Model fits to an OVSA spectrum observed at 17:50:30 UT. The OVSA spectrum is shown as a histogram. Model parameters denoted are: n_{10} (density in units of 10^{10} cm^{-3}), T_6 (temperature in 10^6 K), and B_g (magnetic field in gauss). Top panel: three densities are adopted to show how the spectrum varies with density. Middle panel: the same model parameters as in the top panel are used except that T is raised to 10 times higher. Bottom panel: two models with a weaker (stronger) magnetic fields (dotted and dashed lines) are averaged to give an inhomogeneous model (solid line).

in the top panel) reproduces the high frequency spectrum to some extent, but fails to match the low frequency spectrum. If a homogeneous model predicted a more rapidly increasing spectrum at low frequencies than observed, we may suspect that the disagreement is due to source inhomogeneity in reality (e.g., Lee et al. 1994). In this case, however, the model predicts a more extended spectrum toward lower frequencies than observed. We thus adjusted other factors maintaining the homogeneous source assumption. With a higher densities $7 \times 10^{10} \text{ cm}^{-3}$ the model (solid line) reproduces the low frequency slope under the enhanced Razin suppression. It closely fits to the high frequency spectrum as well, except somewhat excessive fluxes are predicted at the highest observed frequencies. If we further raise the density as desired for supporting the thick target HXR source, we end up with a disagreement between the model (dashed line) and observation at both low and high frequencies, unfortunately.

At this point we should clarify one basic limitation encountered in the current modeling. Even though we will further adjust other parameters to reproduce the microwave spectrum more closely, the density requirement for this microwave spectrum is rather strict. That is, the minimum cut-off frequency for microwave radiation is the local plasma frequency, a sole function of density. More specifically, the o-mode is cut-off at local plasma frequency and x-mode, at a higher frequency that depends on magnetic field as well (Melrose 1980). Since this spectrum starts above 3 GHz, we derive $n \leq 1 \times 10^{11} \text{ cm}^{-3}$. Admittedly this density is a few factor lower than the one needed for explaining the HXR source dimension varying with energy under the CTTM, and this limit value of density cannot be adjusted by change of other parameters.

We now proceed with the ‘lowered’ target value of density. Since the excessive fluxes at high frequencies are due to free-free emission, we adopted higher temperatures as way of suppressing the free-free emission. The three models shown in the middle panel inherit the same parameters from those in the top panel except the temperature increased to $2 \times 10^7 \text{ K}$. At this high temperature, the high frequency fluxes are significantly *reduced*, and all models agree to the observed spectrum at high frequencies. We may further increase temperature without losing this success, but too a high temperature is unwanted in a physical point of view, because the medium should be a cold-target for Coulomb collisions. Emslie (2003) quantified the condition for cold target as $E > 5kT$ where E is the electron energy and T is the target temperature. Kosugi et al. (1988) have shown that the electrons producing photons at ϵ have an energy in the range, $1 < E/\epsilon < 3$. Since we concern ourselves with the RHESSI spectrum above 6 keV, the temperature $2 \times 10^7 \text{ K}$ or 2 keV may qualify as cold target. However, T cannot be much higher than this, especially considering that this photon spectrum is very soft and E could be close to ϵ . For instance, $E/\epsilon < 2$ gives $T < 2.4 \times 10^7 \text{ K}$ for cold target.

In the above, change of the temperature helped to fit the high frequency spectrum, but now these models no longer fit the low frequency spectrum. To come up with this problem, we adjust the magnetic field, B . In general, increasing (decreasing) B results in a shift of the spectrum to higher

(lower) frequencies. Two models calculated with $B = 250$ gauss and 350 gauss are respectively shown as the dotted and dashed lines in the bottom panel. Each individual model spectrum appears to be narrower than the observed spectrum. The low (high) field strength model could, however, reproduce the low (high) frequency spectrum. We thus created an average model (solid line) of these two by linearly summing the flux from each model, which well agrees to the observed spectrum in overall. We thus conclude that the source must have an inhomogeneous magnetic field distribution in the range of $250 \text{ gauss} \leq B \leq 350 \text{ gauss}$. The viewing angle of magnetic field, θ , is another variable and this should be high. Otherwise, the free-free emission tends to compete with the gyrosynchrotron radiation, which is unwanted in this case. An extensive exercise shows that a high viewing angle is preferred, and we have fixed θ to 75° throughout this modeling. All these calculations were made with the isotropic pitch angle distribution of electrons. If it were significantly anisotropic, the resulting spectral morphology may differ from the present result even for the same electron energy distribution. In that case, a few more assumptions regarding the electron energy distribution will be needed, which we do not regard essential for the current study.

5. Concluding Remarks

We have studied the HXR and microwave data of the 2002 September 9 flare with a goal of testing the coronal thick target hypothesis for HXR sources based on the accompanying microwave spectra. Our study found that the microwave spectrum provides strong constraints on the thick target interpretation of HXR sources. First of all, the lowest frequency of the microwave spectrum is strictly determined by the local plasma density, and the derived density $\leq 1 \times 10^{11} \text{ cm}^{-3}$ is close to, but 5 times lower than the density found from the energy dependent variation of the coronal HXR source. Not only the density but temperature $\geq 2 \text{ keV}$ and magnetic field strength, 250–350 gauss, are also required which will again be constrained by the condition for a cold-target for bremsstrahlung and the measurement of the photospheric magnetic field, respectively.

The next question will be whether these constraints could be alleviated by introducing a more realistic, inhomogeneous density structure instead of the simplified assumption for a uniform density source. We commonly consider a source of dense and tenuous regions mixed, i.e., filamentary structure, in which case the tenuous regions filled with nonthermal electrons work as microwave sources and the dense regions, the thick target HXR sources. This scenario is not necessarily promising because microwaves should propagate through the dense plasma and cannot avoid the highly enhanced free-free opacity. The next conceivable structure is an inhomogeneous loop along its length such that a section in loop-top is tenuous, and the rest is filled with dense materials working as a thick target to Coulomb collisions (Xu et al. 2007). This model is actually favorable for explaining the microwave source, but has to be disputed because it is in apparent conflict with the HXR source lying in the loop-

top. In our current idea, the only plausible case would be a somewhat arbitrary coaxial loop structure which consists of the inner loop filled with dense colder plasma and the outer one with tenuous and hot plasma, so that the former is ideal for the thick target HXR source and the latter, more favorable for the microwave emission. In this case the small disagreement between the densities derived from microwaves and HXRs, respectively, could be made acceptable. This scenario would, however, need an explanation as to why the inner core has dense and colder materials compared with the outer part of the loop.

In summary, microwave spectrum provides unique constraints on the coronal HXR sources through the cut-off frequency, the cold target temperature, the free-free opacity, and the Razin effect. These constraints are related to the fundamental physics and are thus robust. Microwave spectral observations should therefore be regarded as a new asset for validating those events of the coronal HXR sources and for determining additional source conditions for them that were not available from HXR observations alone. Future studies may be benefitted from the use of microwave polarizations and time profiles that will further enhance its diagnostic capabilities.

We thank *RHESSI* team for excellent data set. This work was supported by WCU Program through NRF funded by MEST of Korea (R31-10016). J.L. was supported by the International Scholarship of Kyung Hee University, and also by NASA grants, NNX11AB49G and NAS5-01072 (NA03) 937836 to NJIT. G.S.C. was supported by the Korea Research Foundation grant funded by the Korean Government (KRF-2007-313-C00324). M. J. expresses his thanks to Kyung Hee University for granting him a sabbatical, during which his part of this research was performed.

REFERENCES

- Belkora, L. 1997, *ApJ*, 481, 532
Brown, J. C. 1971, *Sol. Phys.*, 18, 489
Dulk, G. A. 1985, *ARA&A*, 23, 169
Emslie, A. G. 2003, *ApJ*, 595, L119
Fleishman, G. D. & Kuznetsov, A. A. 2010, *ApJ*, 721, 1127
Guo, J., Emslie, A. G., Kontar, E. P., et al. 2012a, *A&A*, 543, 53
Guo, J., Emslie, A. G., Massone, A. M., and Piana, M., 2012b, *ApJ* 755, 32
Ji, H., Wang, H., Schmahl, E. J., Qiu, J., Zhang, Y. 2004, *ApJ*, 605, 938
Kosugi, T., Dennis, B. R., & Kai, K, 1988, *ApJ*, 324, 1118
Krucker, S., Hurford, G. J., MacKinnon, A. L., Shih, A. Y., & Lin, R. P. 2008, *ApJ*, 678, 63

- Lee, J. & Gary, D. E. 2000, *ApJ*, 543, 457
- Lee, J., Gary, D. E., & Choe, G. S., 2006, *ApJ*, 647, 638
- Lee, J., Gary, D. E., & Zirin, H. 1994, *Sol. Phys.*, 152, 409
- Piana, M., Massone, A. M., Hurford, G. J., et al. 2007, *ApJ*, 665, 846
- Ramaty, R. 1969, *ApJ*, 158, 753
- Razin, V. A. 1960, *Izv. VUZov. Radiofiz.*, 3, 584
- Sakao, T., Kosugi, T., Masuda, S., Yaji, K., Ina-Koide, M., & Makishima, K. 1996, *AdSpR*, 17, 67
- Sui, L., Holman, G. D., & Dennis, B. R. 2004, *ApJ*, 612, 546
- Melrose, D. B. 1980, *Plasma Astrophysics*, Gordon and Breach, Science Publishers, Inc.
- Veronig, A., and Brown, J. 2004, *ApJ*, 603, L117
- Xu, Y., Emslie, A. G., & Hurford, G. J. 2008, *ApJ*, 673, 576